Atomistic Insights into the Irradiation Effects in Molybdenum

Waqas Akhtar[1] ID, M. Mustafa Azeem[2] * ID, Muhammad Bilal Khan[3] ID
[1]College of Material Science & Engineering, Harbin Institute of Technology, Harbin, 150001, China.
[2]Department of Civil, Architectural, and Environmental Engineering, Missouri University of Science and Technology, Rolla, MO, 65409, USA.
[3]Department of Mechanical Engineering, Ghulam Ishaq Khan Institute of Engineering and Technology, Topi, Swabi 23640, KP, Pakistan.
waqas666@hrbeu.edu.cn[1], ravian20052007@gmail.com[2] *, m.bilalkhan@giki.edu.pk[3]

Abstract— In this study, we examined the impact of energies of 2.54 keV and 5 keV displacement cascades in molybdenum (Mo) using an atomistic simulation at 300 K. The simulation was carried out using machines learning developed spectral neighbor analysis potential (SNAP). We computed displacement threshold energy (E_d), vacancy formation energy (E_v^f), interstitial formation energy (E_i^f), interstitial cluster formation energy (E_{cf}^i), activation energy barrier of interstitial (E_{ai}), activation energy barrier of vacancy (E_{aV}), elastic properties, i.e., shear, bulk, young's modulus, poison ratio. The simulations for primary displacement cascades were performed over a statistical average of 20 independent molecular dynamics simulations such that peak time and the surviving number of defects are inversely proportional to the incident energy of primary knock-on atoms (E_{PKA}). Additionally, it is established that the number of clusters ($N_{clusters}$) during displacement cascades is directly proportional to E_{PKA}. Furthermore, it was revealed that the number of interstitial clusters is higher than the number of vacancy clusters. This research will provide atomic insight into the interactions of defects in Mo for the development of structural materials for high temperature applications.

Keywords—Molecular dynamics, Molybdenum, Primary defect formation, Defect clusters, atomic scale

I. INTRODUCTION

The degradation of materials due to radiation exposure is a significant concern for the safety and reliability of power plants. Extreme conditions primarily change the microstructure of metals and alloys, which is reflected in both their physical and chemical properties. This causes dislocation loops, voids, bubbles, defect clusters, and stacking fault tetrahedra to form and grow [1]. Advanced reactors are fast reactors with state-of-the-art technology having extended service conditions, and they are expected to have a longer life than present technology [2]. The materials have multilayered metallic structures and high radiation stability due to existing interfaces, which can absorb the defects. Keeping this in view, there is an urgent need for novel materials capable of sustaining extreme environments. To understand the material's performance in extreme conditions, the radiation damage response must be meticulously analyzed, both experimentally and computationally [3]. Certain phenomena are difficult to explain experimentally and require integrated simulation and experimental approaches. The study of radiation damage is vital since the current materials in light water reactors (LWR) have materials integrity and safety concerns after Fukushima [4]. Furthermore, the materials used in current reactors are unsuitable for advanced-generation reactors. There are numerous candidate materials for advanced reactors that are suitable for various parts of the plant. Refractory metal alloys are considered candidates for GEN-IV reactors due to their radiation resistance and corrosive nature at higher temperatures [5]. Mo has demonstrated many unique properties suitable for high-temperature applications in advanced fission and fusion reactors, such as T-91 alloys. They have a high melting point and superior radiation resistance to swelling and corrosion in liquid metal coolant environments [6].

It is important to mention that primary radiation damage has been studied by computer simulation quite extensively. Nord et al. reported an extensive review of radiation damage in metallic alloys and explained that atomic simulation methods not only provide the evolution of defects but the mechanism for defects interaction at a very short time scale [7]. It is also worth mentioning that such an approach can be used as a predictive modeling tool for designing better radiation-resistant materials [8]–[16]. The number of observable defects was found to grow nonlinearly with radiation dose [13]. These results suggest that the identified faults are affected by cascade overlap. On the other hand, early MD simulations have demonstrated that if the collision cascade overlaps with pre-existing defects, the number of point defects formed decreases [17].

A crucial component of the worldwide nuclear revival is molybdenum (Mo). Mo attracts a lot of attention since it has numerous distinctive qualities. Due to its high melting point, excellent high-temperature stability, good thermal conductivity,

resistance to radiation-induced swelling, and corrosion resistance in liquid metal coolants, it is appropriate for high-temperature applications in advanced fission and fusion reactor systems. Mo-Fe-Cr alloys are anticipated to play a key role in industrial plants, such as in boilers, cooling towers, process tubes, pumps, and reactors, due to the highly corrosive nature of biofuels.

In this study, we have investigated the effect of irradiation doses on displacement cascades, defect formation energies, and mechanisms for defect interactions in Mo. Displacement cascade simulations were performed at 2.54 keV and 5 keV at 300 K by using the spectral neighbor analysis potential (SNAP). The selection for this energy range is usually reported for displacement cascades in earlier studies. The number of irradiated defects and their growth are plotted as a function of time. We investigated the defects dependence as a function of cascade energies.

II. COMPUTATIONAL METHODOLOGY

Atomic scale simulations were performed by a Large-scale Atomic/Molecular Massively Parallel Simulator (LAMMPS), developed by S. Plimpton [17]. In MD simulations, realistic interatomic potentials are a critical factor in determining the properties under study. In the present study, we used the spectral neighbor analysis potential (SNAP) proposed by Y. Zuo [18]. This interatomic potential is obtained through high-accuracy quantum electronic structure calculations [19]. Furthermore, this potential has been used for investigating Mo properties of large-scale models over longer time scales. In addition, this potential has a reputation for being among the most precise descriptions of defect production energies. The SNAP potential integrates EAM and MEAM potentials replicating their properties as determined through density functional theory [19]. Figure 1 represents the MD snapshot of Mo model. Figure 1 (a) supercell with dimension 10×10×10 containing 2000 atoms with a lattice constant of 3.16 Å. The time step for every simulation is different for each case which will be mentioned for each simulation done in the following section. Thermal relaxations were done using through CG minimization method. Periodic boundaries were set along three dimensions. The initial structure was equilibrated at 300 K with an isobaric isothermal (NPT) ensemble for 15ps. The defects analysis was performed using Wigner-Seitz's method.

For elastic constants, convergence occurs after forces decreased below 10^{-10} eV/Å. The system must be subjected to certain stress-strain ε_{ij}. Each tensor element specifies the magnitude of the deformation in a certain direction, and it makes the values of the elements interrelated. A series of MD simulations were used to calculate the displacement threshold for various E_{PKA} kinetic energies between 50 and 150 eV. The incident PKA was bombarded at 7^0 to avoid the channeling effect [20] at 4 ps. To calculate interstitial formation energies E_i^f ,the time-step was taken to be 0.005ps and counted the total number of atoms in the cell N_o. The initial velocity is established for all atoms based on the steepest descent algorithm, then the cell structure is relaxed, and the initial energy E_i is calculated, and an atom is inserted. After insertion, the system requires

initial energy minimization to achieve a reliable result from MD simulation, and the final energy E_f is calculated as follows.
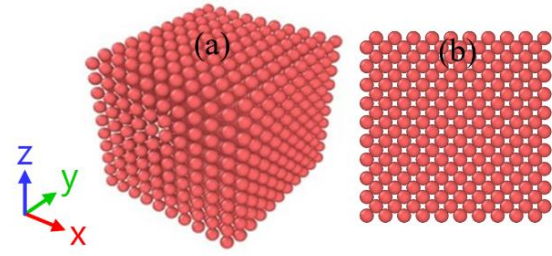

Figure 1. MD snapshot of an initial relaxed model at 300K. (a) A unit cell of Mo (b) 2D snapshot of Mo.

$$E_i^f = E_f - (\frac{N_0+1}{N_0})E_i \qquad (1)$$

$$E_i^f = E_f - (\frac{N_0+1}{N_0})E_i \qquad (2)$$

Similarly, vacancy E_{cf}^v and interstitial cluster formation energy E_{cf}^i are calculated by the above relation. The calculation for E_{cf}^i by inserting two atoms one by one in the lattice of the cell along [110] make a cluster follow the relation, where Nc is the number of clusters.

$$E_{cf}^v = E_f - (\frac{N_0-N_C}{N_0})E_i \qquad (3)$$

$$E_{cf}^v = E_f - (\frac{N_0+N_C}{N_0})E_i \qquad (4)$$

For activation barrier energy, bcc cubic lattice with equal side lengths of $22 \times a_o$. The simulated cell has 21296+N atoms, where N is the interstitial atom that was added to the supercell to make the dumbbell. The migration energy barrier for interstitials is calculated by MD using the NEB method. This algorithm is based on 0 K temperature. Initial and final atomic positions before and after diffusion are located automatically through LAMMPS using minimum energy path (MEP) when a vacancy jumps to a nearby lattice site. For this migration, an atom must become energetic and unlock the atom from its lattice and start a physical transition.

To generate primary cascades of energies, we used a simulation cell having dimensions of $30 \times 30 \times 30 \ nm^3$ and $40 \times 40 \times 40 \ nm^3$ in all three directions was created with a total number of 54000 and 128000 atoms, respectively. For each energy of PKA, the cascade was allowed to evolve over time-steps of a few ps with dt~0.2fs. For each case, 20 independent simulations with various PKA positions and recoil directions were carried out to get statistically meaningful results. The cascade energy was set as 2.54 and 5 KeV. The displacement cascade simulations were carried out using NVE ensemble.

III. RESULTS AND DISCUSSIONS

A. Elastic Properties

In the present simulation, the model was subjected to strain ε_{ij} with tensors along 6×6×6 which deform the model. Each tensor element specifies the magnitude of the deformation in six

independent orientations. The 36 elastic tensor components might be computed by combining the six strains and six stress elements. The calculated results of the simulation are presented in Table 1, where G is shear modulus, K bulk modulus, E is

Properties	Present work	Reference	Units
G	106	106 [21], [22]	GPa
K	258	250-258 [21], [22]	GPa
E	320	315-343 [21]	GPa
v	0.24	0.29 [21]	

young modulus and v represents the poisson ratio.

TABLE I.   COMPUTED ELASTIC PROPERTIES OF MO USING MD.

B. Displacement threshold (E_d)

Figure 2 (a) demonstrated the contour plot of the E_d surface for Mo within a rectangle of non-equivalent crystallographic directions (θ, φ) as calculated by MD simulations. The value of E_d in Mo varies predominantly with E_{PKA}. The range of E_d in Mo is between 50 eV and 98 eV. Such a large energy range is due to the crystal structure and orientation. The values of E_d has a smooth surface in the plane of [111], along the XY plane [110]. E_d much smaller than simply a few degrees off the main direction is quite near to it. For E_d a similar pattern of action is seen at [100]. It can be seen that E_d has the highest values [111] direction, while the minimum one is along the [100]. The mean value of E_d for Mo is estimated to be 60.80 eV which is in good accord with the value determined by the ASTM standard [23]. The minimum value of E_d for Mo is 50 eV, and the maximum value of E_d is 98 eV, which is significantly larger than Fe as reported by Maury [24]. This difference resulted due to the fact E_d values were obtained over 20 different crystallographic directions whereas in our study we simulated 20 directions to take statistical average.

C. Interstitial formation energy (E_v^i)

In the present model, we observed that Mo atom exists in one of the interstitial positions. It can also be thought of as removing one from the atom crystal and moving it to a site interstitial. By using Eq. (1), the interstitial formation energy is calculated to be 8.3514 eV consistent with [25] i.e. 8.20 eV. In Figure 2 (b) the interstitial state is represented in the simulation cell. The energy per atom is displayed in red as peak energy while light blue and white atoms surrounding the red represent low energy. This shift is due to the additional atom being forced into the cell.

D. Vacancy formation energy (E_v^f)

By using (2) amount of vacancy formation energy E_v^f is calculated, which is 2.55 eV, and verified with [26], which was reported as 2.61 eV. Figure 2 (c) displays a vacancy in a simulation cell. The 8 red atoms exhibit the maximum energy because their bonds were broken when the atom was taken out to create the vacancy. Due they weren't connected to the deleted atom and could move because of the void created during thermal relaxation, the four light red atoms had less energy than the red atoms.
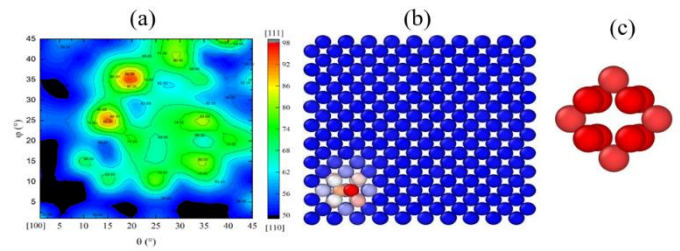

Figure 2 . (a) Contour plot of surface for Mo in the rectangle of crystal direction (θ,φ). The color bar on the side shows energy in eV, (b) Interstitial is visible in a slice of the simulation cells. (c) The vacancy is depicted in a simulation cell

E. Cluster formation energy of vacancy(E_{cf}^v)

By using (3), E_{cf}^v is calculated as 4.96 eV for size one cluster agrees with earlier studies i.e. 4.84 eV [27]. For size two clusters were computed as 7.67 eV and consistent with reported earlier, i.e. 7.28eV [27]. Likewise, the size three and four clusters are calculated as 9.98 eV and 12.56 eV respectively. Figure 3 (a), vacancy clusters are represented in simulation cells different sizes of clusters are demonstrated here. Each atom's color is determined by its energy per atom. Since the bonds with the atom that's been replaced to create the vacancy cluster are broken, the vacancy cluster was formed. Red atoms show the highest amount of energy because they are bound to the atoms that have been removed to make a cluster. Other light red, pink, and light blue atoms had lower energy than the red because they are relocated due to the vacancy clusters to be taken about by the relaxation.

F. Cluster formation of interstitial (E_{cf}^i)

By using (4) E_{cf}^i is calculated for size one cluster was 14.41 eV consistent with 13.78 eV. Similarly, for size with 2 clusters was calculated as 21.73 eV comparable with reported earlier as 20.10 eV, and it is 29 eV for size three and size four clusters 34 eV respectively [28]. The energy per atom gives atoms are presented in different colors as displayed in Figure 3. Red atoms display peak energy. Light blue and white atoms surrounding the red represent low energy than red as they were shifted outward due to the additional atom being forced into the cell.
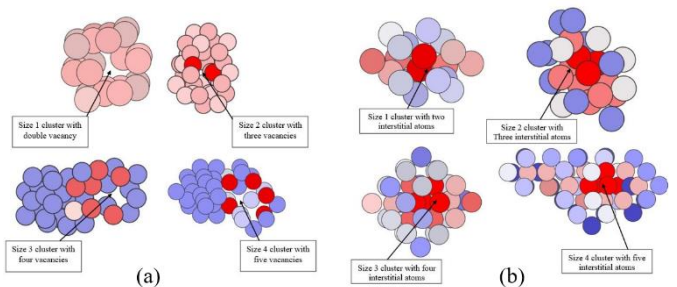

Figure 3. Schematic representation of (a) every single vacancy cluster size 1, 2, 3, 4. (b) every single interstitial cluster of size 1,2,3,4

G. Activation energy barrier of interstitial (E_{ai})

The most stable interstitial defects in metals are dumbbells with two atoms sharing the same lattice site. The diffusion energy barrier, also known as migration energy, is one of the essential characteristics of the diffusion process. In pure Mo, the mechanism of diffusion of ⟨110⟩ orientated dumbbell is presented. The interstitial is rotated along ⟨110⟩ dumbbell and migrates to another ⟨110⟩ interstitial dumbbell on a different plane. The maximum interstitial diffusion barrier energy calculated using the NEB calculations is 2.35 eV viz is in agreement with SNAP results [26], i.e. 2.85 eV. Figure 4 (a) shows the energy barrier as a function of the migration path. The diffusion barrier energy for reorienting a <110> dumbbell to a <111> dumbbell achieved from such studies was considerably lower. It confirmed the theory that the method of <110> interstitial dumbbell migration studied in this study is the most energy-efficient.

H. Activation energy barrier of vacancy (E_{av})

The activation barrier energy was calculated at 1.2916 eV viz in agreement with MD, DFT, and SNAP results, i.e. 1.39 eV [26]. Figure 4 (b) shows the potential barrier for a single vacancy motion curve. Theoretical estimations by Brooks et al., [29], showed that E_v^f in bcc crystals is more than the vacancy barrier energy. The barrier energy computed is compared to E_v^f agrees with Brooks et al. [29]. However, Damask et al. [30] reported no vacancy annealing stage at temperatures corresponding to motion energy of 0.68 eV in a comprehensive study of bcc metals. They suggested a model explain these findings, which implies that vacancies move at a temperature corresponding to motion energy larger than 1.0 eV approximately.
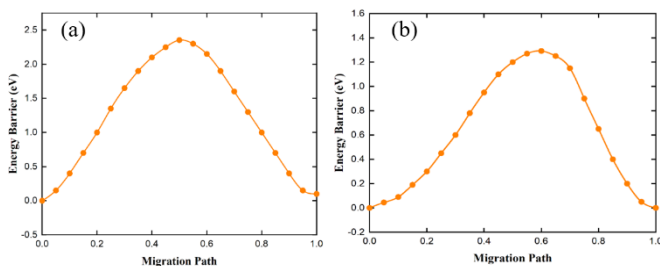

Figure 4. The relationship between energy barrier and migration path for (a) <110>Mo-Mo interstitial atom, (b) <110> Mo vacancy

I. Cascade Overlapping

The results were obtained by running a total of 20 MD cascade simulations for each E_{PKA}. The displacement cascade simulations were performed until the system reached equilibrium. After the initiation of the displacement cascade, we analyzed damage evolution as a function of time. The related temporal behavior of the thermal spike, its lifetime, and the number of defects produced was measured for each given energy. Thus, the usual response of damage evolution over time for 2.54 and 5 KeV E_{PKA} after 20 cumulative recoils of the subject material. In Figure 5 number of defects are proportional to E_{PKA}. However, about the same number of defects, irrespective of the

irradiation energy, are preserved in Mo at the end of the ballistic phase.

We determined the relationship between the number of defects as a time function of 20 cumulative recoils as shown in Figure 5 (b). It illustrates the values of a maximum number of defects are proportional to the energy of incident PKA. However, the rise in the peak number of defects is much faster for low energy than for higher energy. This happens as a result of the initial cascade's dispersal into several smaller cascades, which results in secondary knock-on atoms (SKAs) that have less energy than PKAs [33].

The peak number of defects is directly proportional to the number of cascades. However, this is due to the low defect density cascade core with a smaller number of atomic displacements in separate replacement sequences [8], [10], [15] [31]–[34]. The number of surviving defects leads to radiation-induced microstructural changes. The average number of surviving defects at the end of the simulation (~20 ps) is shown in Figure 5 (a). The number of numbers of surviving pairs versus cascades is displayed in Figure 5 (b). This linear fit follows empirical power law i.e. $N_{FP} = A(E_{PKA})^b$, where, E_{PKA} is the energy of the PKA, and A and b are constants that weakly depended on temperature and lattice structure [35]. As seen in Figure 5 (c), the values of constant A = 2.13 and exponent b = 1.35 for 300 K respectively. Our findings are in good agreement with other molecular dynamics studies on transition metals [36]–[40].
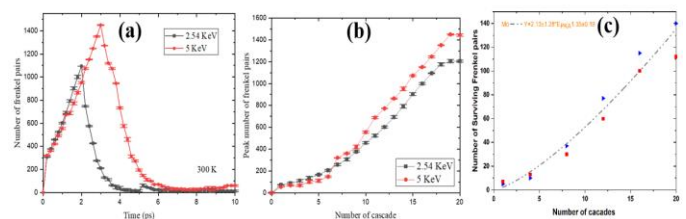

Figure 5. (a) Number of surviving defects as a function of time under different E_{PKA} ,(b) Npeak after 20 cumulative recoils (c) Number of surviving defects as a function of number of cascades at 300 K

The defect density as a function of PKA energy is shown in Figure 6 (a, b), vacancies are denoted in green while interstitials are in blue. The vacancy formation is found to be in the form of sub-clusters in the vicinity of the cascade. However, the interstitials are randomly distributed over a larger distance in the simulation box for each energy [41]. For 2.54 keV and 5 keV PKA energies, vacancy distributions in the form of single clusters and sub-cascades of vacancies are also formed, while interstitial distributions are scattered away from the parent cascade. This results in a larger surface-to-volume ratio and it alternately influences the material property after the damage [42].

When examining irradiation damage, it is useful to know how defects tend to form in-cascade clusters and how larger defect clusters are produced [43]–[45]. Smaller defect clusters act as nuclei for the evolution of longer-lasting defects, which can alter the mechanical properties of the irradiated material [46]. Besides the number of defects produced, the size distribution of vacancies and interstitial clusters as a function of PKA energy

was also studied, as shown in Figure 6 (c, d). It is to be noted that the probability of vacancy and interstitial clustering fraction increases quickly with E_{PKA} as the damage cascade transition from a single displacement cascade to sub-cascade morphology. The number of interstitial clusters surpasses the number of cluster vacancies. If vacancy clusters are stable, they can expand into voids and cavities, both of which are important microstructure features [14]. Our result display that the stability of vacancy clusters is lower than that of interstitial clusters [47]. Therefore, the probability of interstitials forming clusters is greater than the probability of vacancy defects clusters which is an important factor in determining the mechanical properties of radiated materials [48].
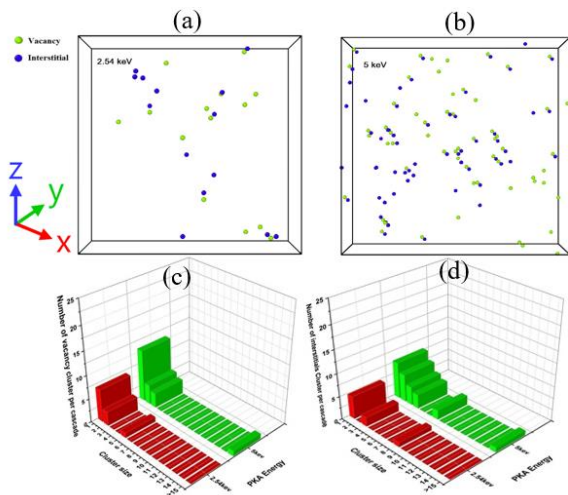
Figures 6. Defect evolution as a function of (a) 2.5keV (b) 5keV, (c) vacancy clusters as a function of energy (d) interstitial clusters as a function of energy.

CONCLUSION

This study has explored the effects of displacement cascades and energy of incident E_{PKA} on the defect evolution in Mo at an operating temperature of a power plant. We explored that Mo exhibits a very high elastic modulus, stiffness, higher strength, and ductility. In addition, displacement cascade simulations were investigated over 2.54 and 5 keV. It was established that the energy of incident PKA is proportional to the number of surviving defects and the size of defect clusters. During thermal spike, we found that a large number of atoms reside in cascades. This cascade propagation led to a large number of surviving point defects and hence permanent damage within the material after the cascade subsides. Furthermore, a clustering study showed that interstitial and vacancy clusters behaved differently, with an increase in the cluster and size distribution for interstitials and a drop for vacancy clusters. Our study will provide atomic insight into developing better radiation-resistant materials.

REFERENCES

[1]   G. S. Was and P. L. Andresen, "G. S. Was and P. L. Andresen, Radiation damage to structural alloys in nuclear power plants: Mechanisms and remediation. 2014.," *Mech. Remediat.*, 2014.

[2]   P. M. Raole and S. P. Deshpande, "Structural materials for fusion reactors," *Trans. Indian Inst. Met.*, vol. 62, no. 2, pp. 105–111, 2009, doi: 10.1007/s12666-009-0014-0.

[3]   S. J. Zinkle and G. S. Was, 'Materials challenges in nuclear energy,' Acta Mater., vol. 61, no. 3, pp. 735– 758, 2013, doi: 10.1016/j.actamat.2012.11.004."

[4]   H. G. Kim, J. H. Yang, W. J. Kim, and Y. H. Koo, "Development Status of Accident-tolerant Fuel for Light Water Reactors in Korea," *Nucl. Eng. Technol.*, vol. 48, no. 1, pp. 1–15, 2016, doi: 10.1016/j.net.2015.11.011.

[5]   S. P. Chakraborty, S. Banerjee, I. G. Sharma, and A. K. Suri, 'Development of silicide coating over Molybdenum based refractory alloy and its characterization,' J. Nucl. Mater., vol. 403, . 1–3, pp. 152–159, 2010, doi: 10.1016/j.jnucmat.2010.06.014."

[6]   T.H. Webster, B.L. Eyre, E.A. Terry, Irradiation Embrittlement and Creep in Fuel Cladding and Core Components, The British Nuclear Energy Society, London, 1972."

[7]   K. Nordlund, A. . Sand, F. Granberg, S. . Zinkle, and R. Stoller, "Primary Radiation Damage in Materials Review: Review of Current Understanding and Proposed New Standard Displacement Damage Model to Incorporate in Cascade Defect Production Efficiency and Mixing Effects," *Oecd/Nea*, vol. NEA/NSC/DO, 2015.

[8]   A. M. Mustafa, Z. Li, and L. Shao, "Molecular Dynamics Simulations of Damage Cascades Creation in Oxide-Particle-Embedded Fe.," in *25th International Conference on Nuclear Engineering, ASME*, 2017, vol. 5, pp. 1–5, doi: 10.1115/ICONE25-67356.

[9]   M. M. Azeem, D. Yun, and M. Zubair, "Atomic insights on interaction mechanism of dislocation with void/impurity/ precipitates in bcc iron," *Int. Conf. Nucl. Eng. Proceedings, ICONE*, vol. 2, pp. 1–7, 2021, doi: 10.1115/ICONE28-65197.

[10]   M. M. Azeem, Q. Wang, Z. Li, and Y. Zhang, "Dislocation-oxide interaction in Y2O3 embedded Fe: A molecular dynamics simulation study," *Nucl. Eng. Technol.*, vol. 52, no. 2, pp. 337–343, 2020, doi: 10.1016/j.net.2019.07.011.

[11]   M. M. Azeem, Q. Wang, and M. Zubair, "Atomistic simulations of nanoindentation response of irradiation defects in iron," *Sains Malaysiana*, vol. 48, no. 9, pp. 2029–2039, 2019, doi: 10.17576/jsm-2019-4809-24.

[12]   M. M. Azeem, Q. Wang, Y. Zhang, S. Liu, and M. Zubair, "Effect of Grain Boundary on Diffusion of P in Alpha-Fe: A Molecular Dynamics Study," *Front. Phys.*, vol. 7, no. 97, pp. 1–7, 2019, doi: 10.3389/fphy.2019.00097.

[13]   M. Mustafa Azeem, K. Abd El Gawad, M. Zubair, S. A. Ibrahim, M. Ado, and G. Mehdi, "Radiation damage effects in oxide dispersion strengthened steel alloys," in *International Conference on Nuclear Engineering, Proceedings, ICONE*, 2019, doi: 10.1299/jsmeicone.2019.27.2086.

[14]   M. M. Azeem, Z. Li, Q. Wang, and M. Zubair, "Molecular dynamics studies and irradiation effects in ODSS alloys," *Int. J. Nucl. Energy Sci. Technol.*, vol. 12, no. 4, pp. 381–399, 2018, doi: 10.1504/IJNEST.2018.10018247.

[15]   M. M. Azeem, Z. Li, Q. Wang, Q. M. N. Amjad, M. Zubair, and O. M. H. Ahmed, "Classical molecular dynamics study for defect sink behavior in oxide dispersed strengthened alloys," in *Proceedings of 2018 15th International Bhurban Conference on Applied Sciences and Technology, IBCAST 2018*, 2018, pp. 12–15, doi: 10.1109/IBCAST.2018.8312177.

[16]   M. M. Azeem, Z. Li, Q. Wang, and A. Hussian, "Molecular Dynamics Simulation Study on the Possible Factors Affecting Stability of ODS Steel," in *IOP Conference Series: Materials Science and Engineering*, Jul. 2018, vol. 389, p. 012003, doi: 10.1088/1757-899X/389/1/012003.

[17]   Plimpton S."Fast parallel algorithms for short-range molecular dynamics", . Journal of computational physics, 1995, 117(1): 1-19."

[18]   Y. Zuo, C. Chen, X. Li, Z. Deng, Y. Chen, J. Behler, G. Csányi, A.V. Shapeev, A.P. Thompson, M.A. Wood, and S.P. Ong (2020), 'Performance and Cost Assessment of Machine Learning Interatomic Potentials', The Journal of Physical Chemistry A, 124(4), 731-745."

[19]   C. Chen, Z. Deng, R. Tran, H. Tang, I. H. Chu, and S. P. Ong, 'Accurate force field for molybdenum by machine learning large materials data,' Phys. Rev. Mater., vol. 1, no. 4, pp. 1–10, 2017, doi: 10.1103/PhysRevMaterials.1.043603."

[20] N. V Doan and R. Vascon, "Displacement cascades in metals and ordered alloys. Molecular dynamics simulations," *Nucl. Instruments Methods Phys. Res. Sect. B Beam Interact. with Mater. Atoms*, vol. 135, no. 1, pp. 207–213, 1998, doi: 10.1016/S0168-583X(97)00653-8.

[21] S. Zheng and S. Wang, "First-principles design of refractory high entropy alloy VMoNbTaW," *Entropy*, vol. 20, no. 12, 2018, doi: 10.3390/e20120965.

[22] P. C. De Camargo, F. R. Brotzen, and S. Steinemann, "Thermal expansion and elastic properties of Nb-Mo alloys," *J. Phys. F Met. Phys.*, vol. 17, no. 5, pp. 1065–1079, 1987, doi: 10.1088/0305-4608/17/5/008.

[23] A. M. Ougouag, C. A. Wemple, and C. D. Van Siclen, "Displacement Kerma Cross Sections For Neutron Interactions In Molybdenum," 2004.

[24] Maury F, Vajda P, Biget M. Anisotropy of the displacement energy in single crystals of molybdenum[J]. Radiation Effects, 1975, 25(3): 175–185."

[25] "Pramana J. Phys., Vol. 72, No. 5. Self-interstitial configuration in molybdenum studied by modified analytical embedded atom method."

[26] M. J. Norgett, M. T. Robinson, and I. M. Torrens, 'A proposed method of calculating displacement dose rates,' Nucl. Eng. Des., vol. 33, no. 1, pp. 50–54, 1975, doi: 10.1016/0029-5493(75)90035-7."

[27] Hong J, Hu Z, Probert M. disulphide monolayers[J]. Nature Communications, Nature Publishing Group, 2015, 6: 1–8."

[28] S. V Starikov *et al.*, "Radiation-induced damage and evolution of defects in Mo," *Phys. Rev. B - Condens. Matter Mater. Phys.*, vol. 84, no. 10, pp. 1–8, 2011, doi: 10.1103/PhysRevB.84.104109.

[29] Azároff L V. Role of Crystal Structure in Diffusion. I. Diffusion Paths in Closest-Packed Crystals[J]. Journal of Applied Physics, 32(9), 1658–1662.1961."

[30] Sizmann R. The effect of radiation upon diffusion in metals[J]. Journal of Nuclear Materials, Volumes 69: 386–412."

[31] Heald P N K & P T. Point defects in molybdenum[J]. Philosophical Magazine, 1974: 1137–1147."

[32] Dehlinger U. Solid State Physics. Physical Review Materials, 1956, 9: 1–139."

[33] L. Bukonte, T. Ahlgren and K H. Modelling of monovacancy diffusion in W over wide temperature range. Applied Physics, 2014."

[34] Ma, P.-W., & DUDAREV S L. Effect of stress on vacancy formation and migration in body-centered-cubic metals[J]. Physical Review Materials, 2019, 3."

[35] Q. U. A. Sahi and Y. S. Kim, "Primary radiation damage characterization of α-iron under irradiation temperature for various PKA energies," *Mater. Res. Express*, vol. 5, no. 4, 2018, doi: 10.1088/2053-1591/aabb6f.

[36] M. J. Demkowicz, P. Bellon, and B. D. Wirth, "Atomic-scale design of radiation-tolerant nanocomposites," *MRS Bull.*, vol. 35, no. 12, pp. 992–998, 2010, doi: 10.1557/mrs2010.704.

[37] D. H. R. R.E. H. Clark, *Nuclear Fusion Research understanding plasma-surface*. 2005.

[38] C. S. Becquart and C. Domain, "Modeling microstructure and irradiation effects," *Metall. Mater. Trans. A*, vol. 42, no. 4, pp. 852–870, 2011, doi: 10.1007/s11661-010-0460-7.

[39] G. S. Was *et al.*, "Emulation of reactor irradiation damage using ion beams," *Scr. Mater.*, vol. 88, 2014, doi: 10.1016/j.scriptamat.2014.06.003.

[40] J. B. GIBSON, A. N. GOLAND, M. MILGRAM and G H V. Dynamics of Radiation Damage[J]. Physical Review, 1960, 120."

[41] C. P. Chui, W. Liu, Y. Xu, and Y. Zhou, "Molecular Dynamics Simulation of Iron - A Review," *Spin*, vol. 5, no. 4, pp. 1–36, 2015, doi: 10.1142/S201032471540007X.

[42] N. P. Lazarev and A. S. Bakai, "Atomistic simulation of primary damages in Fe, Ni and Zr," *J. Supercrit. Fluids*, vol. 82, pp. 22–26, 2013, doi: 10.1016/j.supflu.2013.06.002.

[43] C. S. Becquart *et al.*, "Modeling the long-term evolution of the primary damage in ferritic alloys using coarse-grained methods," *J. Nucl. Mater.*, vol. 406, no. 1, pp. 39–54, 2010, doi: 10.1016/j.jnucmat.2010.05.019.

[44] O. El-Atwani, J. E. Nathaniel, A. C. Leff, K. Hattar, and M. L. Taheri, "Direct Observation of Sink-Dependent Defect Evolution in Nanocrystalline Iron under Irradiation," *Sci. Rep.*, vol. 7, no. 1, pp. 1–12, 2017, doi: 10.1038/s41598-017-01744-x.

[45] E. G. Hayward, "Atomistic Studies of Defects in Bcc Iron: Dislocations and Gas Bubbles," no. August, 2012.

[46] R. E. Stoller, "Role of cascade energy and temperature in primary defect formation in iron," *J. Nucl. Mater.*, vol. 276, no. 1, pp. 22–32, 2000, doi: 10.1016/S0022-3115(99)00204-4.

[47] Y.N. Osetsky, D. Bacon, V. Mohles, Atomic modelling of strengthening mechanisms due to voids and copper precipitates in α-iron, Philosophical magazine, 83 (2003) 3623-3641."

[48] K. P. Zolnikov, A. V. Korchuganov, and D. S. Kryzhevich, "Molecular dynamics simulation of primary radiation damage in Fe-Cr alloy," *J. Phys. Conf. Ser.*, vol. 774, no. 1, 2016, doi: 10.1088/1742-6596/774/1/012130.

Waqas Akhtar born in Pakistan.Currently , he is pursuing PhD in Material Science and Engineering from Harbin Institute of technology's Harbin, Heilongjiang, China. He completed Master's degree in Nuclear Engineering from Harbin Engineering University Harbin, Heilongjiang, China on fully funded scholarship in 2021. His research interests focus on atomic scale modellingat extreme condtions.

How to cite this article: